Monthly Notices
of the
ROYAL ASTRONOMICAL SOCIETY

MNRAS **432,** 3228–3236 (2013)
Advance Access publication 2013 May 21

doi:10.1093/mnras/stt680

Signatures of pulsars in the light curves of newly formed supernova remnants

K. Kotera,[1,2]★ E. S. Phinney[2] and A. V. Olinto[3]

[1]*Institut d'Astrophysique de Paris, UMR7095 - CNRS, Université Pierre & Marie Curie, 98 bis boulevard Arago, F-75014 Paris, France*
[2]*California Institute of Technology, Mailcode 350-17, 1200 East California Boulevard, Pasadena, CA 91125, USA*
[3]*Department of Astronomy & Astrophysics, Kavli Institute for Cosmological Physics, The University of Chicago, Chicago, IL 60637, USA*

Accepted 2013 April 17. Received 2013 April 16; in original form 2013 February 13

ABSTRACT

We explore the effect of pulsars, in particular those born with millisecond periods, on their surrounding supernova ejectas. While they spin down, fast-spinning pulsars release their tremendous rotational energy in the form of a relativistic magnetized wind that can affect the dynamics and luminosity of the supernova. We estimate the thermal and non-thermal radiations expected from these specific objects, concentrating at times a few years after the onset of the explosion. We find that the bolometric light curves present a high luminosity plateau (that can reach 10^{43}–10^{44} erg s^{-1}) over a few years. An equally bright TeV gamma-ray emission, and a milder X-ray peak (of the order of 10^{40}–10^{42} erg s^{-1}) could also appear a few months to a few years after the explosion, as the pulsar wind nebula emerges, depending on the injection parameters. The observations of these signatures by following the emission of a large number of supernovae could have important implications for the understanding of core-collapse supernovae and reveal the nature of the remnant compact object.

Key words: pulsars: general – supernovae: general – gamma-rays: general – X-rays: general.

1 INTRODUCTION

Core-collapse supernovae (SNe) are triggered by the collapse and explosion of massive stars, and lead to the formation of black holes or neutron stars (see e.g. Woosley, Heger & Weaver 2002). In particular, pulsars (highly magnetized, fast rotating neutron stars) are believed to be commonly produced in such events. The observed light curves of core-collapse SNe present a wide variety of shapes, durations and luminosities which many studies have endeavoured to model, considering the progenitor mass, explosion energy, radioactive nucleosynthesis and radiation transfer mechanisms in the ejecta (e.g. Hamuy 2003; Baklanov, Blinnikov & Pavlyuk 2005; Utrobin & Chugai 2008; Kasen & Woosley 2009).

While they spin down, pulsars release their rotational energy in the form of a relativistic magnetized wind. The effects of a central pulsar on the early SN dynamics and luminosity is usually neglected, as the energy supplied by the star is negligible compared to the explosion energy, for the bulk of their population. Some pioneering works have, however, sketched these effects (Pacini & Salvati 1973; Gaffet 1977a,b; Bandiera, Pacini & Salvati 1984; Reynolds & Chevalier 1984), notably in the case of SN 1987A (McCray, Shull & Sutherland 1987; Xu et al. 1988). More recently, Kasen & Bildsten (2010) and Dessart et al. (2012) discussed that magnetars, a subclass of pulsars born with extremely high dipole magnetic fields of the order of $B \sim 10^{14}$–10^{15} G and millisecond spin periods, could deposit their rotational energy into the surrounding SN ejecta in a few days. This mechanism would considerably brighten the SN, and could provide an explanation to the observed superluminous SNe (Quimby 2012).

In this paper, we explore the effects of mildly magnetized pulsars born with millisecond periods (such as the Crab pulsar at birth) on the light curves of the early SN ejecta. Such objects are expected to inject their tremendous rotational energy in the SN ejecta, but over longer times compared to magnetars (of the order of a few years). Indeed, the spin-down and thus the time-scale for rotational energy deposition is governed by the magnetization of the star.

We estimate the thermal and non-thermal radiations expected from these specific objects, concentrating at times of a few years after the onset of the explosion. We find that the bolometric light curves present a high luminosity plateau (that can reach 10^{43}–10^{44} erg s^{-1}) over a few years, and that an equally bright TeV gamma-ray emission could also appear after a few months to a few years, from the acceleration of particles in the pulsar wind, depending on the injection parameters. A milder associated X-ray peak (of luminosity 10^{40}–10^{42} erg s^{-1}) could also be produced around the same time. The observations of these signatures by the following up of a large number of SNe could have important implications for the understanding of core-collapse SNe and reveal the nature of the remnant compact object.

★E-mail: kotera@iap.fr

These objects also present an ideal combination of parameters for successful production of ultrahigh energy cosmic rays (UHECRs, see Blasi, Epstein & Olinto 2000; Fang, Kotera & Olinto 2012). The observation of such SNe could thus be a further argument in favour of millisecond pulsars as sources of UHECRs, and a potential signature of an ongoing UHECR production.

We first give, in Section 2, the list of quantities necessary for this analysis in the regimes of interest for the ejecta, optically thin or thick, and present a scheme of the early interaction between the pulsar wind and the SN ejecta. In Section 3, we calculate the bolometric, thermal and non-thermal light curves of our peculiar SNe. In Section 5, we briefly discuss available observations and the implications for UHECR production.

2 SUPERNOVA EJECTA HOSTING A MILLISECOND PULSAR: PROPERTIES

We note $M_{\rm ej}$ and $E_{\rm ej}$ as the mass and initial energy of the SN ejecta. The pulsar has an inertial momentum I, radius R_*, initial rotation velocity $\Omega_{\rm i}$ (corresponding initial period $P_{\rm i} = 2\pi/\Omega_{\rm i}$) and dipole magnetic field B. Numerical quantities are noted $Q_x \equiv Q/10^x$ in cgs units, unless specified otherwise.

2.1 Time-scales

For an ordinary core-collapse SN, the ejecta expands into the circumstellar medium at a characteristic final velocity

$$v_{\rm ej} = v_{\rm SN} = \left(2\frac{E_{\rm ej}}{M_{\rm ej}}\right)^{1/2} \sim 4.5\times10^{8}\,{\rm cm\,s^{-1}}\,E_{\rm ej,51}^{1/2}M_{\rm ej,5}^{-1/2}, \quad (1)$$

where $M_{\rm ej,\,5} \equiv M_{\rm ej}/5\,{\rm M}_\odot$. After a few expansion time-scales $t_{\rm ex} = R_{\rm ej,\,i}/v_{\rm SN}$, where $R_{\rm ej,\,i}$ is the radius of the star that led to the explosion, the ejecta enters into a stage of homologous expansion where its size scales as $R = v_{\rm ej}t$ and its internal energy as $E_{\rm int}(t) \sim (E_{\rm ej}/2)(t_{\rm ex}/t)$.

The ejecta is first optically thick to electron scattering. Noting κ and ρ the opacity and density of the SN envelope, one can estimate the optical depth of the ejecta: $\tau = R\kappa\rho$. Assuming a constant central SN density profile (see Matzner & McKee 1999 and Chevalier 2005 for more detailed modelling of the interior structure of SNe) $\rho = 3M_{\rm ej}/(4\pi R^3)$, one can define the effective diffusion time (for thermal photons to cross the ejecta) as

$$t_{\rm d} \equiv \left(\frac{M_{\rm ej}\kappa}{4\pi v_{\rm ej}c}\right)^{1/2} \quad (2)$$

$$\sim 1.6\times10^{6}\,{\rm s}\,M_{\rm ej,5}^{1/2}\kappa_{0.2}^{1/2}\left(\frac{v_{\rm ej}}{2\times10^{9}\,{\rm cm\,s^{-1}}}\right)^{-1/2}, \quad (3)$$

with the opacity to electron scattering defined as $\kappa_{0.2} \equiv \kappa/(0.2\,{\rm g^{-1}\,cm^2})$ for thermal photons. This sets the time-scale of the SN light curve, under the assumption that the opacity remains constant throughout the ejecta (no ionization effect), and in the absence of pulsar or ^{56}Ni heating. For a more detailed computation of these time-scales, see e.g. Kasen & Woosley (2009).

As the ejecta expands, it reaches a time $t_{\rm thin}$ when it becomes optically thin to electron scattering, for thermal photons ($\tau = 1$):

$$t_{\rm thin} = \left(\frac{3M_{\rm ej}\kappa}{4\pi v_{\rm ej}^2}\right)^{1/2} \sim 1.9\times10^{7}\,{\rm s}\left(\frac{v_{\rm ej}}{2\times10^{9}\,{\rm cm\,s^{-1}}}\right). \quad (4)$$

For the numerical estimates of $v_{\rm ej}$, we are using the final velocity of the ejecta after its modification by the shock at the interface between the pulsar wind and the initial ejecta, for $E_{\rm ej,\,51}$, $M_{\rm ej,\,5}$ and $P_{\rm i} = 10^{-3}$ s (see equation 8 in Section 2.2).

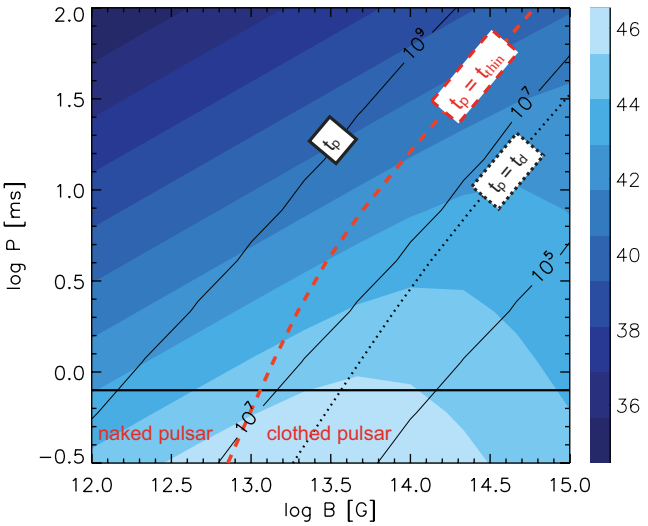

Figure 1. Contour plot of the bolometric luminosity of SN+PWN systems at 1 yr after the explosion (the fraction of wind energy converted into radiation, as defined in Section 3, is set to $\eta_\gamma = 1$), as a function of the initial period P and magnetic field B. The various regimes for radiative emissions described in Section 2.1 are represented. The solid lines indicate the pulsar spin-down time-scale in seconds (equation 5). The red dashed lines represent the pulsar population for which $t_{\rm p} = t_{\rm thin}$, and separate naked and clothed pulsars (see text). The dotted lines represent $t_{\rm p} = t_{\rm d}$.

The pulsar spins down by electromagnetic energy losses that are transferred to the surrounding environment. The deposition of this energy happens over the spin-down time-scale of the pulsar (Shapiro & Teukolsky 1983):

$$t_{\rm p} = \frac{9Ic^3}{2B^2R_*^6\Omega_{\rm i}^2} \sim 3.1\times10^{7}\,{\rm s}\,I_{45}B_{13}^{-2}R_{*,6}^{-6}P_{\rm i,-3}^{2}. \quad (5)$$

We will consider two regimes for the calculation of radiative emissions from the ejecta: optically thin ($t > t_{\rm thin}$) and optically thick ($t < t_{\rm thin}$) for thermal photons. The deposition of pulsar rotational energy will have different effects on the SN radiative emissions according to the optical depth of the ejecta at time $t_{\rm p}$. Fig. 1 pictures these various regimes. The red dashed lines represent the pulsar population for which $t_{\rm p} = t_{\rm thin}$: on its left-hand side, most of the rotational energy of the pulsar is injected when the SN ejecta is optically thin to electron scattering (the pulsar is *naked*). On the right-hand side of the red dashed line, the pulsar energy can enhance the luminosity of the SN, as it is injected while the ejecta is still optically thick (the pulsar is *clothed*).

2.2 Characteristics of the SN ejecta and of the embedded pulsar wind nebula

The interaction between the pulsar wind and the SN ejecta leads to the formation of the following structures, illustrated in Fig. 2: a forward shock at the interface between the shocked and unshocked ejectas, and a reverse shock at the interface between the shocked and unshocked wind (commonly called the 'termination shock'). The shocked material between the forward and the reverse shocks constitutes the pulsar wind nebula (PWN, e.g. Chevalier 1977; Chevalier & Fransson 1992; Gaensler & Slane 2006).

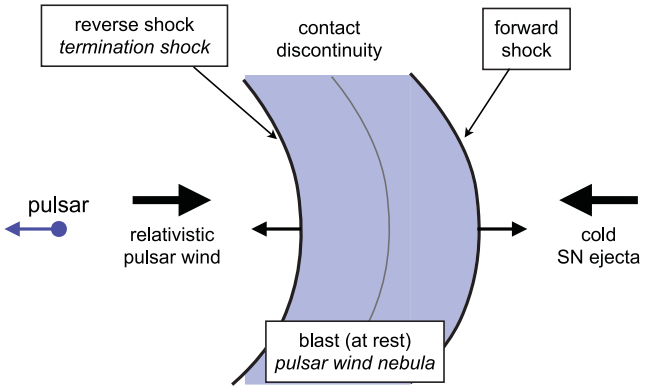

Figure 2. Scheme of the structures created by the interaction between the pulsar wind and the SN ejecta in the blast rest mass frame.

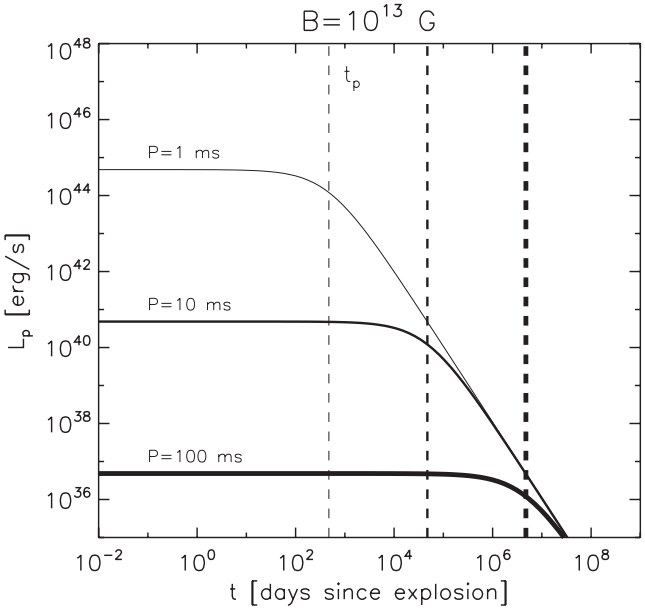

Figure 3. Evolution of the pulsar luminosity L_p as a function of time, for magnetic dipole spin-down. The pulsar has a dipole magnetic field of $B = 10^{13}$ G, and a period $P_i = 1, 10, 100$ ms (increasing thickness). The vertical dashed lines correspond to the spin-down time-scale t_p for each initial spin period.

The pulsar wind carries a total energy of

$$E_p = \frac{I\Omega_i^2}{2} \sim 1.9 \times 10^{52}\,\mathrm{erg}\, I_{45} P_{i,-3}^2 \tag{6}$$

and injects a luminosity (Shapiro & Teukolsky 1983) of

$$L_p(t) = \frac{E_p}{t_p}\frac{1}{(1+t/t_p)^2} \tag{7}$$

into the cold SN ejecta. The evolution of the pulsar luminosity over time, for magnetic dipole spin-down, is represented in Fig. 3.

The characteristic velocity of the ejecta is not affected by the PWN expansion if $E_p \ll E_{ej}$. However, if the pulsar input energy overwhelms the initial ejecta energy, $E_p \gg E_{ej}$, the ejecta is swept up into the shell at a final shell velocity $v_f = (2E_p/M_{ej})^{1/2}$ (Chevalier 2005). Taking into account these two extreme cases, one can estimate the characteristic ejecta velocity as

$$v_{ej} = v_{SN}(1 + E_p/E_{SN})^{1/2}. \tag{8}$$

For $E_p \ll E_{ej}$, the evolution of the PWN takes place in the central part of the SN ejecta, where the density profile is nearly flat, with $\rho \propto t^{-3}(r/t)^{-m}$. We will assume here that $m = 0$. For times $t \le t_p$ where $L_p \sim E_p/t_p$, the radius of the PWN can then be expressed as (Chevalier 1977)

$$R_{PWN} \sim \left(\frac{125}{99}\frac{v_{ej}^3 E_p}{M_{ej} t_p}\right)^{1/5} t^{6/5}, \text{ for } t \le t_p,\ E_p \ll E_{ej}. \tag{9}$$

Beyond the characteristic velocity v_{SN}, the density profile of the ejecta steepens considerably, reaching spectral indices $b \gtrsim 5$ (e.g. Matzner & McKee 1999). For $E_p \gg E_{ej}$, the PWN expands past this inflection point and its size depends on whether the swept-up shell breaks up by Rayleigh–Taylor instabilities. Chevalier (2005) discusses that if the shell does not break up, the expansion is determined by the acceleration of a shell of fixed mass; thus, for $t \le t_p, E_p \gg E_{ej}$ andnoshelldisruption

$$R_{PWN} = \left(\frac{8}{15}\frac{E_p}{M_{ej} t_p}\right)^{1/2} t^{3/2} \tag{10}$$

$$\sim 2.2 \times 10^{16}\,\mathrm{cm}\, E_{p,52}^{1/2} M_{ej,5}^{-1/2} t_{p,yr} \quad \text{for } t = t_p. \tag{11}$$

Otherwise, the evolution of the nebula is set by pressure equilibrium, and $R_{PWN} \propto t^{(6-b)/(5-b)}$ (for $t < t_p, E_p \gg E_{ej}$). In the following, because the fate of the shell is unclear at this stage, we will use equation (10) as an illustration.

For $t > t_p$, L_p drops, and the swept-up material tends towards free expansion. One can roughly assume the relation

$$R_{PWN}(t > t_p) = R_{PWN}(t_p)\frac{t}{t_p}, \tag{12}$$

where $R_{PWN}(t_p)$ is the size of the PWN in equations 9 and 10. More detailed modellings of the dynamical evolution of pulsar-driven SN remnants (SNRs) can be found in Reynolds & Chevalier (1984).

The magnetic field strength in the PWN can then be estimated assuming a fraction of magnetization η_B of the luminosity injected by the wind (see Fig. 4):

$$B_{PWN} = \left(8\pi\eta_B \int_0^t L_p(t')\mathrm{d}t'\right)^{1/2} R_{PWN}(t)^{-3/2}. \tag{13}$$

The value of η_B could vary between 0.01 and 1, according to PWNe.

3 BOLOMETRIC RADIATION

In what follows, we calculate the total radiation expected from the SN ejecta+PWN. The evolution of the ejecta is computed assuming a one-zone core-collapse model. This approximation is debatable for times $t \lesssim t_d$, as the radiation should be mainly emitted in the central regions, close to the PWN, and not uniformly distributed as the matter over a single shell. This is not expected to be limiting for our study, however, as we are most interested in the late-time light curves (a few years after the explosion), when the ejecta starts to become optically thin.

How much energy of the pulsar wind will be transformed into radiation depends on many factors such as the nature of the wind (leptonic, hadronic or Poynting flux dominated), and the efficiency of particle acceleration and radiative processes. In a first step, these conditions can be parametrized by setting a fraction η_γ of the wind energy E_p that is converted to radiative energy (thermal or non-thermal) in the PWN.

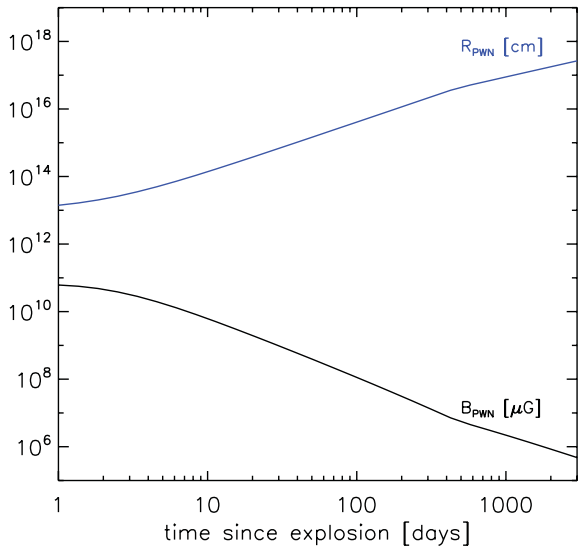

Figure 4. Evolution in time of the radius, $R_{\rm PWN}$, and the magnetic field strength, $B_{\rm PWN}$, of a PWN, assuming no shell disruption (equations 10 and 12) and $\eta_B = 0.01$, calculated for an SN ejecta with $M_{\rm ej} = 5\,{\rm M}_\odot$ and $E_{\rm ej} = 10^{51}$ erg s^{-1}, embedding a pulsar with a dipole magnetic field of $B = 10^{13}$ G and period $P_{\rm i} = 1$ ms.

Under the one-zone-model approximation, the radiation pressure dominates throughout the remnant, $P = E_{\rm int}/3V$, with V the volume of the ejecta. The internal energy then follows the law

$$\frac{1}{t}\frac{\partial}{\partial t}[E_{\rm int} t] = \eta_\gamma L_{\rm p}(t) - L_{\rm rad}(t). \quad (14)$$

The radiated luminosity $L_{\rm rad}$ depends on the ejecta optical depth:

$$\frac{L_{\rm rad}(t)}{4\pi R^2} = \frac{E_{\rm int} c}{(4\pi/3) R^3} \quad t > t_{\rm thin} \quad (15)$$

$$= \frac{E_{\rm int} c}{(4\pi/3)\tau R^3} \quad t \leq t_{\rm thin} \quad (16)$$

which yields

$$L_{\rm rad}(t) = \frac{3}{\beta_{\rm ej}}\frac{E_{\rm int}}{t} \quad t > t_{\rm thin} \quad (17)$$

$$= \frac{E_{\rm int} t}{t_{\rm d}^2} \quad t \leq t_{\rm thin} \quad (18)$$

where we note $\beta_{\rm ej} \equiv v_{\rm ej}/c$. For $t < t_{\rm thin}$, we assumed that the totality of the luminosity $\eta_\gamma L_{\rm p}$ deposited in the ejecta as photons is thermalized, and used the diffusion transport approximation (Arnett 1980). In the optically-thin regime, photons do not diffuse and propagate straight out of the ejecta.

Equation (14) yields

$$E_{\rm int}(t) = \frac{\eta_\gamma E_{\rm p}}{1 + 3/\beta_{\rm ej}}\left[h_1\left(\frac{t}{t_{\rm p}}\right) - h_2\left(\frac{t}{t_{\rm p}}\right)\right], \quad t > t_{\rm thin} \quad (19)$$

$$= \frac{1}{t} {\rm e}^{-\frac{t^2}{2t_{\rm d}^2}} \left[\int_{t_{\rm ex}}^{t} {\rm e}^{\frac{x^2}{2t_{\rm d}^2}} \frac{\eta_\gamma E_{\rm p} t_{\rm p} x}{(t_{\rm p} + x)^2} {\rm d}x + E_{\rm ej}\, t_{\rm ex}\, {\rm e}^{\frac{t_{\rm ex}^2}{2t_{\rm d}^2}}\right], \quad t \leq t_{\rm thin}. \quad (20)$$

The hypergeometric functions are noted:

$$h_1(x) \equiv {}_2F_1(1, 1 + 3/\beta_{\rm ej}, 2 + 3/\beta_{\rm ej}, -x), \quad (21)$$

$$h_2(x) \equiv {}_2F_1(2, 1 + 3\beta_{\rm ej}, 2 + 3/\beta_{\rm ej}, -x)\,. \quad (22)$$

Note that $L_{\rm rad}(t) \sim \eta_\gamma L_{\rm p}(t)$ for $t > t_{\rm thin}$.

To calculate the total bolometric radiated luminosity, we add to $L_{\rm rad}(t)$ the contribution of the ordinary core-collapse SN radiation $L_{\rm SN}(t)$. $L_{\rm SN}(t)$ is calculated following equation (5) of Chatzopoulos, Wheeler & Vinko (2012), assuming an initial luminosity output of 10^{42} erg s^{-1}, as is estimated by Woosley et al. (2002) in their equation (41), for $M_{\rm ej} = 5\,{\rm M}_\odot$ and $E_{\rm ej} = 10^{51}$ erg s^{-1}. $L_{\rm SN}$ only contributes when $E_{\rm p} < E_{\rm SN}$.

Fig. 5 presents the bolometric luminosity radiated from the ejecta+PWN system for various sets of pulsar parameters. Again, the Arnett (1980) approximation is not necessarily valid for $t < t_{\rm d}$, where the radiation should not be distributed over the whole ejecta. Even with a $\eta_\gamma < 10$ per cent, the plateau in the light curve a few years after the explosion is highly luminous, especially for $P = 1$ ms. This high luminosity plateau stems from the injection of the bulk of the pulsar rotational energy a few years after the SN explosion. The luminosity is quickly suppressed for high B (for magnetar-type objects), due to the fast spin-down. SNe embedding isolated millisecond pulsars with standard magnetic field strengths would thus present unique radiative features observable a few years after their birth.

Note, however, that the luminosity represented here is the bolometric one. The emission should shift from quasi-thermal to high energy after a few years, depending on the evolution of the opacity of the ejecta. The emission at different energies is discussed in the next section.

4 THERMAL/NON-THERMAL EMISSIONS

The bolometric radiation calculated in the previous section stems from the reprocessing of high-energy radiation created at the base of the SN ejecta, in the PWN region. In the standard picture of the PWN, high-energy particles (leptons and hadrons) are injected at the interface between the pulsar wind and the ejecta, and radiate high-energy photons (X-rays and gamma-rays). These high-energy photons can be either thermalized if the medium (the PWN and/or the SN ejecta) is optically thick to these wavelengths or can escape from the ejecta and be observed as a high-energy emission, if the medium they have to propagate through is optically thin. In this section, we calculate in more detail the emission a few years after the explosion, concentrating mainly on the case of a leptonic wind.

Upstream of the termination shock, the energy of the pulsar wind is distributed between electrons and positrons, and ions and magnetic fields. The fraction of energy imparted to particles is not certain, especially at these early times. Near the neutron star, the Poynting flux is likely to be the dominant component of the outflow energy. After many hundreds of years, observational evidence show that the energy repartition at the termination shock of PWNe is dominated by particles (e.g. Arons 2007). The conventional picture is thus that all but ∼0.3–1 per cent of the Poynting flux has already been converted into the plasma kinetic energy by the time the flow arrives the termination shock (Kennel & Coroniti 1984a,b; Emmering & Chevalier 1987; Begelman & Li 1992), ∼1 per cent appearing to be the level required to reproduce the observed shape of the Crab nebula (Del Zanna, Amato & Bucciantini 2004; Komissarov & Lyubarsky 2004). How this transfer happens is a subject of debate (see e.g. Kirk, Lyubarsky & Petri 2009).

Particles and the Poynting flux are injected in the PWN at the termination shock. We will note the energy repartition between

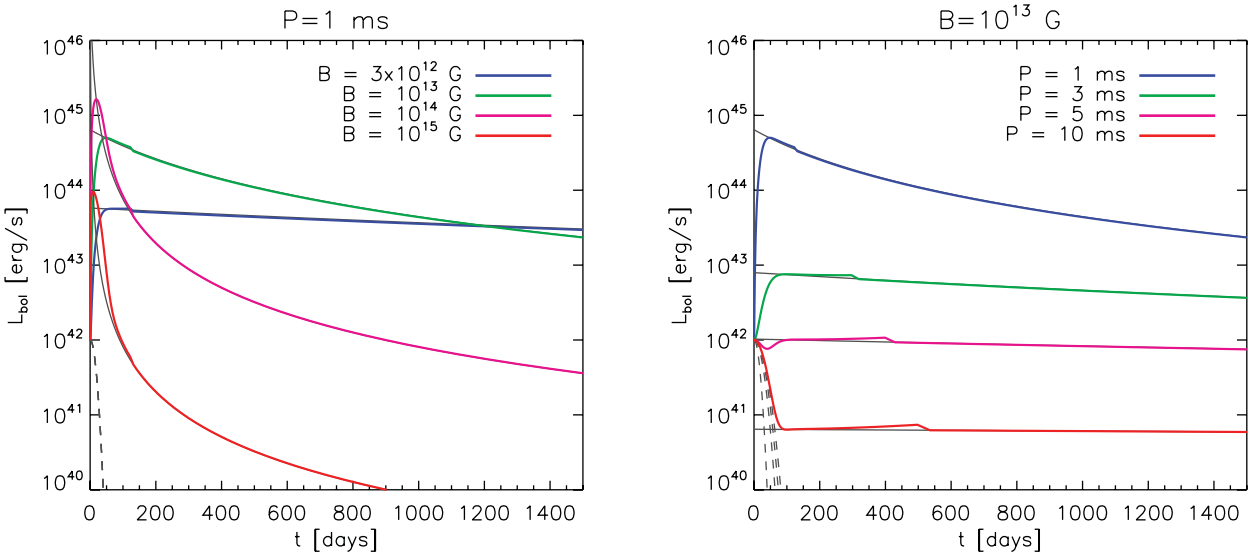

Figure 5. Evolution of the bolometric radiated luminosity of the SN as a function of time. The pulsar has a dipole magnetic field of increasing strength as indicated, and a period $P_i = 1$ ms (left-hand panel), and $B = 10^{13}$ G and increasing periods as indicated in the legend (right-hand panel). The SN ejecta has $M_{ej} = 5\,M_\odot$ and $E_{ej} = 10^{51}$ erg. The grey lines give the evolution of the pulsar luminosity L_p for each initial spin period. The grey dashed lines are the contribution of the ordinary core-collapse SN to the radiated luminosity L_{SN}. We have assumed $\eta_\gamma = 1$. The slight discontinuity is due to the numerical calculation of the integral in equation (20), and marks the transition between $t < t_{thin}$ and $t < t_{thin}$.

electrons and positrons, and ions and the magnetic field in the PWN: $L_p = (\eta_e + \eta_i + \eta_B)L_p$. The ratio between η_i and η_e is the subject of another debate (see e.g. Kirk et al. 2009). However, various authors (e.g. Gelfand, Slane & Zhang 2009; Fang & Zhang 2010; Bucciantini, Arons & Amato 2011; Tanaka & Takahara 2011) seem to fit satisfactorily the observed emissions for various late-time PWNe without adding any hadronic injection. We will thus focus on the emission produced for winds dominated by a leptonic component at the termination shock.

Note that if protons are energetically dominant in the wind, Amato, Guetta & Blasi (2003) calculated that a large flux of neutrinos, gamma-rays and secondary pairs from p–p pion production should be expected from Crab-like PWNe around a few years after the SN explosion. They estimate that the synchrotron emission from secondaries will be negligible, while the TeV photon and neutrino emission could be detectable by current instruments if such young objects were present in our Galaxy.

Only 1 per cent of the relativistic ions and magnetic field components of the wind can be converted into thermal energy in the ejecta (Chevalier 1977). This fraction can be amplified in the presence of, e.g. Rayleigh–Taylor mixing, or high-energy cosmic-ray diffusion into the ejecta.

4.1 Pair injection in the PWN

According to the original idea by Kennel & Coroniti (1984a), the pair injection spectrum into the PWN should present a Maxwellian distribution due to the transformation of the bulk of the kinetic energy of the wind into thermal energy, and a non-thermal power-law tail formed by pairs accelerated at the shock. Hybrid and particle-in-cell simulations have indeed shown such a behaviour (e.g. Bennett & Ellison 1995; Spitkovsky 2008; Dieckmann & Bret 2009). Spitkovsky (2008) finds that 1 per cent of the particles are present in this tail, with 10 per cent of the total injected energy. The bulk of the particle energy would then be concentrated around the kinetic energy upstream of the termination shock:

$$\epsilon_b = kT_e = \gamma_w m_e c^2 \tag{23}$$

$$\sim 5 \times 10^{11}\ \mathrm{eV}\ \frac{\gamma_w}{10^6}, \tag{24}$$

with γ_w the Lorentz factor of the wind. The non-thermal tail would start around ϵ_b and continue up to higher energies with a spectral index $\gtrsim 2$. In practice, from a theoretical point of view, Lorentz factors as high as $\gamma_w \sim 10^6$ are difficult to reach, and current simulations are only capable of producing γ_w of the order of a few hundreds (Spitkovsky 2008; Sironi & Spitkovsky 2009).

However, observationally, various authors (Kennel & Coroniti 1984a, but also more recently, e.g. Gelfand et al. 2009; Fang & Zhang 2010; Bucciantini et al. 2011; Tanaka & Takahara 2011) demonstrated that the non-thermal radiation produced by the injection of either one single power law or a broken power law peaking around $\epsilon_b \sim 1$ TeV, and extending up to PeV energies, could fit successfully the observed emission of various young PWNe. Such a high break energy implies either a high Lorentz factor for the wind $\gamma_w \sim 10^5$–10^6, or an efficient acceleration mechanism enabling particles to reach 0.1–1 TeV energies. At higher energies, another acceleration mechanism has to be invoked to produce particles up to PeV energies. Bucciantini et al. (2011) discuss that ϵ_b could possibly be viewed as a transition energy between Type II and Type I Fermi acceleration from low to high energies. This would provide a physical explanation to the broken-power-law shape, and alleviate the issue of the high wind Lorentz factor. At high energies, acceleration could also happen in the course of reconnection of the striped magnetic field in the wind, at the termination shock (Lyubarsky 2003; Pétri & Lyubarsky 2007). However, it is not clear yet whether this process can lead to a non-thermal particle distribution. One can expect additional particle acceleration in the wind itself, via surf-riding acceleration (Arons 2002, 2003; Chen, Tajima & Takahashi 2002; Contopoulos & Kazanas 2002). This non-thermal component would not necessarily be processed when injected at the shocks if the particle Larmor radii are large compared to the size of the shock.

In the following, we will assume that pairs are injected in the PWN following a broken power law of the form

$$\frac{\mathrm{d}\dot{N}}{\mathrm{d}\epsilon}(\epsilon,t) = \frac{\eta_\mathrm{e} L_\mathrm{p}(t)}{\epsilon_\mathrm{b}^2} \begin{cases} (\epsilon/\epsilon_\mathrm{b})^{-\alpha} & \text{if} \quad \epsilon_\mathrm{min} \le \epsilon < \epsilon_\mathrm{b} \\ (\epsilon/\epsilon_\mathrm{b})^{-\beta} & \text{if} \quad \epsilon_\mathrm{b} \le \epsilon \le \epsilon_\mathrm{max} \end{cases} \tag{25}$$

where $\alpha < 2 < \beta$, ϵ_min and ϵ_max are the minimum and maximum cut-off energies, respectively, and ϵ_b is the peak of the injection distribution, $\epsilon(\mathrm{d}N/\mathrm{d}\epsilon) \sim 0.1$–$1$ TeV. It is commonly assumed that $\epsilon_\mathrm{b} \propto \gamma_\mathrm{w} \propto \sqrt{L_\mathrm{p}(t)}$, but such an assumption would imply very high wind Lorentz factors ($>10^9$) at early times which seem incompatible with the simulations and theoretical models discussed above. It is likely that the Lorentz factor experiences a saturation above a certain value, and for simplicity, we will assume that ϵ_b is constant over time. For our purpose of deriving a rough estimate of the fraction of high-energy emission that can escape the ejecta at early times, such an approximation will suffice. A thorough calculation of the emission spectrum would require time-dependent energy-loss calculations for particles beyond the one-zone approximation that we use here. Del Zanna et al. (2004, 2006) have shown indeed that the high-energy emission is strongly affected by the details of the flow dynamics just downstream of the termination shock.

4.2 Radiation by accelerated pairs

The bulk of the electron distribution will predominantly radiate in synchrotron and experience inverse Compton (IC) scattering off the produced synchrotron photons. The cooling time-scales of these processes, as well as the dynamical time-scale $t_\mathrm{dyn} = R_\mathrm{PWN}/c$ of the PWN, are indicated in Fig. 6. IC scattering off the thermal photons of the ejecta and off the cosmic microwave background is negligible compared to the former two processes. Fig. 6 also demonstrates that the cooling time-scale of IC scattering off the thermal photons of the SN ejecta is much longer than the time-scale for self-Comptonization of the synchrotron emission. This estimate includes only the contribution of the thermal photons of the standard SN ejecta, as the thermalization of the non-thermal components described here happens on larger time-scales, in the optically-thin regime which is of interest to us.

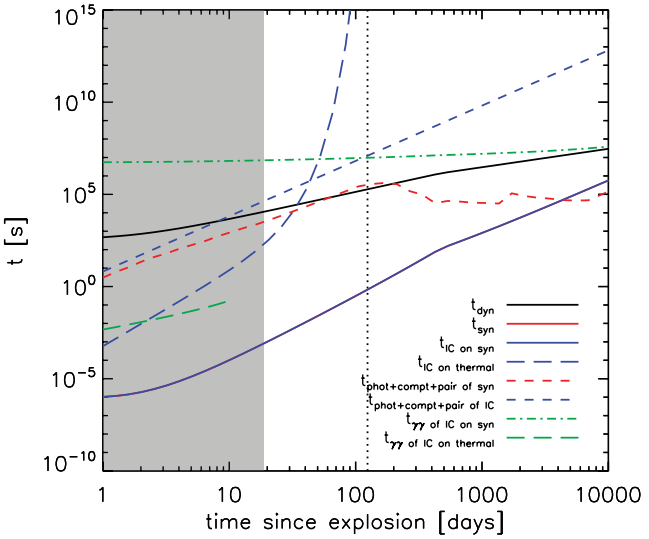

Figure 6. Time-scales at play in the radiation emission of a PWN, for the same system as in Fig. 4, assuming an electron injection break energy $\epsilon_\mathrm{b} = 0.1$ TeV, and $\eta_B = 0.01$. The dynamical time-scale, t_dyn (black solid line), and cooling time-scales via synchrotron, t_syn (red solid line), via self-Compton, $t_\mathrm{IC,\,syn}$ (blue solid line) and via IC off thermal photons (blue long-dashed line) are compared to thermalization time-scales. The thermalization time-scales via photoelectric absorption, Compton scattering and pair production are shown in the dashed lines (in red for the synchrotron photons and blue for the IC photons). Absorption by γ–γ interaction at high energies is shown in the green lines (dot–dashed for the interaction between IC photons on synchrotron photons, and long-dashed for the interaction of IC photons on the thermal photons of the SN ejecta). The grey shaded region corresponds to $t < t_\mathrm{d}$, where the Arnett (1980) approximation is not valid, and the dotted line indicates $t = t_\mathrm{thin}$.

The synchrotron cooling time-scale of accelerated electrons reads

$$t_\mathrm{syn} = \frac{3 m_\mathrm{e}^2 c^3}{4 \sigma_\mathrm{T} \epsilon_\mathrm{c} U_B}\,, \tag{26}$$

with $U_B = B_\mathrm{PWN}^2/8\pi$. At the early stages that we consider here, the characteristic energy of radiating particles is $\epsilon_\mathrm{c}(t) = \epsilon_\mathrm{b}$. The characteristic synchrotron radiation frequency can be expressed as

$$\nu_\mathrm{c}(t) = 0.29 \frac{3 e B_\mathrm{PWN}(t)}{4\pi m_\mathrm{e}^3 c^5} \epsilon_\mathrm{c}^2. \tag{27}$$

Accelerated electrons also scatter off these synchrotron photons by IC, producing photons at energy

$$\nu_\mathrm{IC} = \nu_\mathrm{KN} \equiv \frac{m_\mathrm{e} c^2}{\gamma_\mathrm{e} h} \quad \text{if } \nu_\mathrm{c} > \nu_\mathrm{KN}, \tag{28}$$

$$= \nu_\mathrm{c} \quad \text{if } \nu_\mathrm{c} \le \nu_\mathrm{KN}, \tag{29}$$

with a cooling time-scale

$$t_\mathrm{IC,syn} = \frac{3 m_\mathrm{e}^2 c^4}{4 \sigma_\mathrm{T} c \epsilon_\mathrm{c} U_\mathrm{syn}}, \tag{30}$$

where U_syn is the synchrotron photon energy density. Electrons radiate in synchrotron and self-Compton processes with the following power ratio: $P_\mathrm{IC}/P_\mathrm{syn} = U_\mathrm{syn}/U_B$. Assuming that the energy of the accelerated electron population is concentrated in its peak energy ϵ_b, it implies synchrotron and IC luminosities of $L_\mathrm{syn} = \eta_B \eta_\mathrm{e}/(\eta_B + \eta_\mathrm{e}) L_\mathrm{p}$ and $L_\mathrm{IC} = \eta_\mathrm{e}^2/(\eta_B + \eta_\mathrm{e}) L_\mathrm{p}$, respectively. Obviously, the value of η_B has an impact on the synchrotron emission, but not on the IC emission.

Fig. 7 presents the evolution in time of the luminosities L_p, L_syn and L_IC, as well as the emission frequencies ν_c and ν_IC. The IC radiation is mostly emitted at the break energy of the injection of electrons. The synchrotron emission spans from gamma-ray/X-ray (until a few years) to optical wavelengths (after thousands of years). At the time of interest in this study, X-rays are thus mainly emitted between 0.1 and 100 keV for $\epsilon_\mathrm{b} = 0.1$ TeV, and between around 100 keV and 1 GeV for $\epsilon_\mathrm{b} = 1$ TeV.

4.3 Thermalization in the ejecta

The X-ray opacity (∼0.1–100 keV) is dominated by photoelectric absorption in metals. Above ∼100 keV, very hard X-rays and gamma-rays experience predominantly Compton scattering, and pair production above ∼10 MeV. The opacities of these processes for various atomic media are given in Fig. 8. At a given time t, the optical depth of the ejecta to the characteristic synchrotron photon emission ν_c reads

$$\tau_\mathrm{syn}(t) = v_\mathrm{ej} t \kappa_{\nu_\mathrm{c}}(t) \rho(t). \tag{31}$$

The dominant thermalization process for the TeV IC radiation is pair production by γ–γ interactions (see Fig. 6). The time-scale for thermalization via this process is, however, slightly longer than the

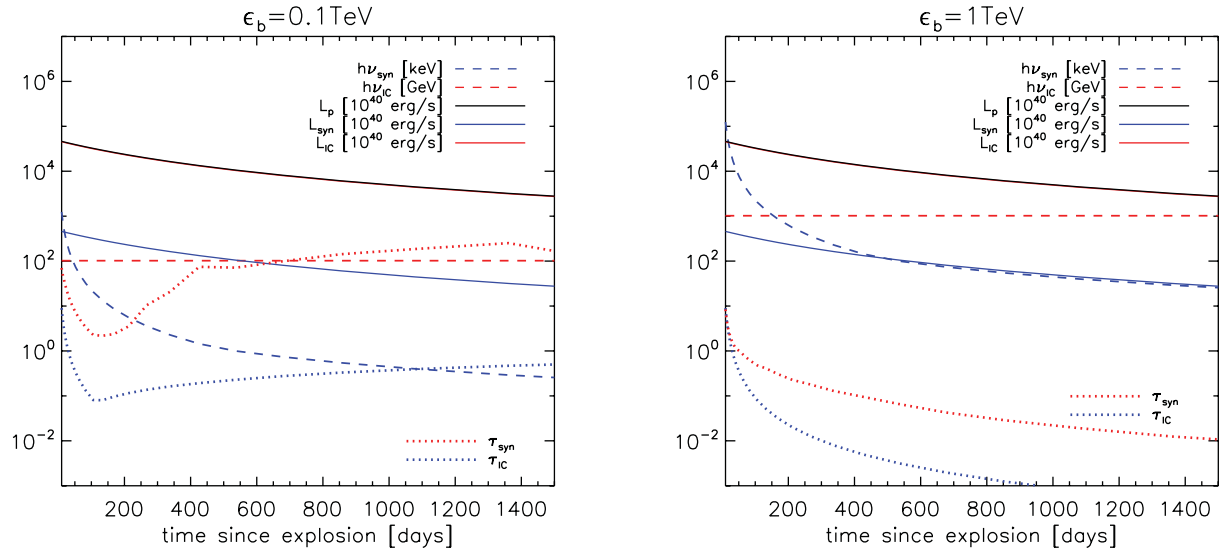

Figure 7. Evolution in time of radiative quantities of the same system as in Fig. 4, with $\eta_B = 0.01$, $\eta_e = 1 - \eta_B$, and for a particle injection break energy of $\epsilon_b =$ 0.1 TeV (left-hand panel) and $\epsilon_b = 1$ TeV (right-hand panel). Blue dashed line: characteristic energy of synchrotron radiation; red dashed lines: characteristic energy of photons produced via self-Comptonization of synchrotron photons. Thin black solid line: luminosity injected by the pulsar. Red and blue solid lines: luminosity emitted in synchrotron and IC radiations. Dotted blue line: optical depth of the ejecta of composition 60 per cent H, 30 per cent He and 10 per cent C to photons of energy $h\nu_c$. Dotted red line: optical depth of the ejecta to photons of energy ν_{IC}.

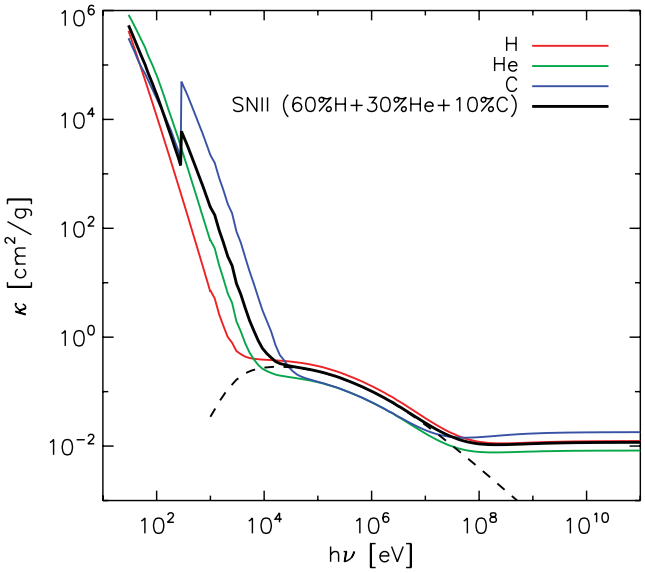

Figure 8. Atomic scattering opacities of high-energy photons on H, He, C and a mixture of composition mimicking that of a Type II core-collapse SN ejecta (60 per cent H, 30 per cent He and 10 per cent C). The black dashed line indicates the contribution of Compton scattering in the latter composition case. From http://henke.lbl.gov/optical_constants/ for 30 eV $\leq h\nu <$ 1 keV and http://physics.nist.gov/cgi-bin/Xcom/ for 1 keV $\leq h\nu <$ 100 GeV.

dynamical time; hence, the ejecta appears mostly optically thin to this radiation (see Fig. 7). We note τ_{IC} for the optical depth of the ejecta to the IC emission.

The luminosity in the characteristic energies $h\nu_c$ and $h\nu_{IC}$ after thermalization, noted, respectively, $L_X(t)$ and $L_\gamma(t)$, and the luminosity in thermal photons, $L_{th}(t)$, are calculated as follows:

$$L_X(t) = L_{syn}(\nu_c, t)\, e^{-\tau_{syn}(t)}, \tag{32}$$

$$L_\gamma(t) = L_{IC}(\nu_{IC}, t)\, e^{-\tau_{IC}(t)}, \tag{33}$$

$$L_{th}(t) = L_{rad}(t) - L_X(t) - L_\gamma(t). \tag{34}$$

Fig. 9 presents the thermal emission (black line), X-ray emission (blue dotted line) at $h\nu_c \sim 0.1$–100 keV for $\epsilon_b = 0.1$ TeV (left-hand panel) and ∼100 keV–1 GeV for $\epsilon_b = 1$ TeV (right-hand panel), and 0.1–1 TeV gamma-ray emission (red dashed line) expected from an SN ejecta with $M_{ej} = 5\,M_\odot$ and $E_{ej} = 10^{51}$ erg s^{-1}, embedding a pulsar with dipole magnetic field of $B = 10^{13}$ G and period $P_i = 1$, 3, 10 ms (increasing thickness), assuming $\eta_B = 0.01$, $\eta_e = 1 - \eta_B$, and a break energy $\epsilon_b = 0.1$ TeV (left-hand panel) and $\epsilon_b = 1$ TeV (right-hand panel).

A decrease in flux is expected in the thermal component after a few months to years, when the ejecta becomes optically thin to gamma-rays. For a low break energy ($\epsilon_b = 0.1$ TeV), the thermal component can then recover, as the X-ray emission vanishes, because of the increase of the ejecta optical depth for lower energy photons. One robust result is that, in both break energy cases, for fast pulsar rotation periods $P_i \leq 3$ ms, the associated gamma-ray flux around 0.1–1 TeV emerges at a level that should be detectable at a few tens of Mpc, and remains strong over many years.

5 DISCUSSION AND CONCLUSION

We have estimated the thermal and non-thermal radiations expected from SN ejectas embedding pulsars born with millisecond periods, concentrating at times a few years after the onset of the explosion. The bolometric light curves should present a high luminosity plateau (that can reach $>10^{43}$ erg s^{-1}) over a few years. A more detailed emission calculation considering the acceleration of leptons in the PWN region shows that an X-ray and a particularly bright TeV gamma-ray emission (of magnitude comparable to the thermal peak) should appear around 1 year after the explosion. This non-thermal emission would indicate the emergence of the PWN from the SN ejecta.

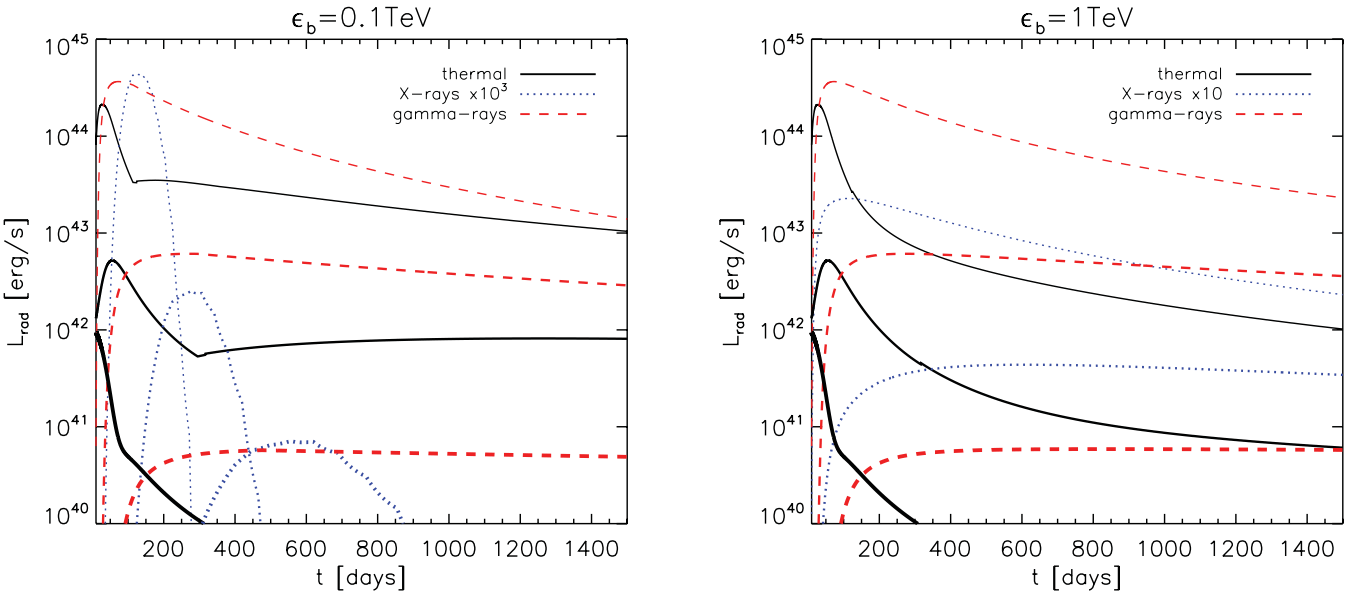

Figure 9. Thermal emission (black solid lines), non-thermal X-ray emission (blue dotted line) at energy indicated in Fig. 7 (emitted mostly between 0.1 and 100 keV for $\epsilon_b = 0.1$ TeV, and between around 100 keV and 1 GeV for $\epsilon_b = 1$ TeV), and non-thermal gamma-ray emission (red dashed line) at 0.1 TeV (left-hand panel) and 1 TeV (right-hand panel), expected from an SN ejecta with $M_{ej} = 5\,M_\odot$ and $E_{ej} = 10^{51}$ erg s^{-1}, embedding a pulsar with a dipole magnetic field of $B = 10^{13}$ G and period $P_i = 1, 3, 10$ ms (increasing thickness), assuming $\eta_B = 0.01$, $\eta_e = 1 - \eta_B$ and a break energy $\epsilon_b = 0.1$ TeV (left-hand panel) and $\epsilon_b = 1$ TeV (right-hand panel). Caution: for visibility, the X-ray luminosity is multiplied by 10^3 in the left-hand panel and by 10 in the right-hand panel. The slight discontinuities are numerical artefacts.

The light curves calculated in this paper are simple estimates which do not take into account second-order effects of radioactive decay of ^{56}Ni, recombination, etc. (see e.g. Kasen & Woosley 2009). The non-thermal components are also evaluated assuming that all the leptonic energy is concentrated in one energy bin. A more detailed analysis should be conducted, taking into account the shape of the spectra and its evolution in time, in order to get a more accurate representation of the emission, and for a thorough comparison with observational data. Depending on the spectral indices, a non-monoenergetic electron injection spectrum could lead to a decrease of the peak luminosity of one order of magnitude.

Our computation of the evolution of the PWN (radius, magnetic field) is also basic, and could benefit from more thorough estimations. Our toy model suffices, however, in the scope of this study, where the aim is to demonstrate the importance of multiwavelength follow-ups of SN light curves. We also assumed a relatively high magnetization η_B of the wind at the termination shock, following estimates that reproduce the features of the Crab nebula (Del Zanna et al. 2004; Komissarov & Lyubarsky 2004).

Several earlier works treat some of the aspects invoked above in more detail. For example, in the context of the evolution of PWNe, early works by Pacini & Salvati (1973), Rees & Gunn (1974), Bandiera et al. (1984), Weiler & Panagia (1980) and Reynolds & Chevalier (1984) take into account the detailed evolution of the particle energy distribution and radiation spectrum. Most of these works aim at calculating radiation features of observed plerions, a few hundreds of years after the explosion. However, their modelling at earlier times, especially in the work of Reynolds & Chevalier (1984), lays the ground for the more detailed calculations that should be performed in our framework.

The level of synchrotron emission predicted here can thus be viewed as optimistic values. However, the gamma-ray flux that is predicted does not depend on the magnetization, and remains fairly robust to most parameter changes.

Currently, only a handful of SNe have been followed over a period longer than a year, and no object, except for SN 1987A, has been examined in X-rays or TeV gamma-rays a year after the explosion. Among the objects that have been followed in optical bands, SN 2003ma (Rest et al. 2011) has an abnormally bright luminosity at the peak, and a long bright tail over many years. The six Type II SNe followed by Otsuka et al. (2012) present various shapes of light curves, and a cut-off in the thermal emission after a few years. Our study demonstrates that the features in these light curves could also be due to the energy injection from the pulsar which could compete with the other processes that are more commonly considered, such as the light echo of the peak luminosity, or the radioactive decay of ^{56}Ni. An associated X-ray and TeV gamma-ray emission emerging around a few months to a year after the explosion would constitute a clear signature of pulsar rotational energy injection. It is also interesting to note that the emergence of a PWN has been recently reported from radio observations for SN 1986J (Bietenholz, Bartel & Rupen 2010), though over longer time-scales than predicted for the objects studied in this paper.

Some authors (Katz, Sapir & Waxman 2011; Murase et al. 2011; Svirski, Nakar & Sari 2012) have discussed that shock breakouts from stars surrounded by a thick wind could lead to a bright X-ray peak after a few months, similar to the signal discussed in this paper. This degeneracy can be overcome by the observation of the gamma-ray signal, which should be absent in the shock breakout scenario. Detailed analysis of the respective X-ray spectra should also help distinguish the two scenarios.

The follow-up of bright Type II SNe over a few years after the explosion in different wave bands would thus reveal crucial information on the nature of the compact remnant. These surveys should be made possible with the advent of optical instruments such as LSST, and the use of powerful instruments for transient event detection, such as the Palomar Transient Factory or Pan-STARR. The bright X-ray signal should be detected by NuSTAR for SNe out to redshifts

$z \sim 0.5$, and the even brighter gamma-ray signal could be observed by HESS2, by the future Cerenkov Telescope Array (CTA), and by HAWK which will be the choice instrument to explore the transient sky at these energies. For CTA, an adequate survey of the sky outside the Galactic plane could spot gamma-ray sources of luminosity 10^{43} erg s^{-1}, as predicted by this work, within a radius of $\sim$150 Mpc (G. Dubus, private communication). Assuming a Gaussian pulsar period distribution centred around 300 ms as in Faucher-Giguère & Kaspi (2006) implies that 0.3 per cent of the total population have spin periods <6 ms. With this estimate, one could find four bright sources within 150 Mpc. This is consistent with the numbers quoted in early works by Srinivasan, Dwarakanath & Bhattacharya (1984) and Bhattacharya (1990). These authors estimated the birthrate of Crab-like pulsar-driven SNRs to be of the order of 1 per 240 years in our Galaxy.

Pulsars born with millisecond periods embedded in standard core-collapse SN ejectas, as described in this paper, are promising candidate sources for UHECRs (Fang et al. 2012; Fang, Kotera & Olinto 2013). In the framework of UHECRs, an injection of the order of 1 per cent of the Goldreich–Julian density into ions would suffice to account for the observed flux, assuming that 1 per cent of Type II SNe give birth to pulsars with the right characteristics to produce UHECRs (i.e. pulsars born with millisecond periods and magnetic fields $B \sim 10^{12-13}$ G, Fang et al. 2012). The observation of the peculiar light curves predicted here could thus provide a signature for the production of UHECRs in these objects. Though no spatial correlation between arrival directions of UHECRs and these SNe is expected (because of time delays induced by deflections in magnetic fields), an indication of the birth rate of these SNe could already give direct constraints on this source model. Photo-disintegration and spallation of accelerated nuclei in the SN ejecta could also lead to an abundant high-energy neutrino production (Murase, Mészáros & Zhang 2009 consider such a neutrino production in the case of magnetars instead of fast-rotating pulsars) which could be detected with IceCube, and correlated with the position of identified peculiar SNe.

ACKNOWLEDGEMENTS

We thank L. Dessart, G. Dubus, M. Lemoine, K. Murase, E. Nakar and J. Vink for very fruitful discussions. KK was supported at Caltech by a Sherman Fairchild Fellowship, and acknowledges financial support from PNHE. AVO was supported through the NSF grant PHY-1068696 at the University of Chicago, through the NSF grant PHY-1125897 at the Kavli Institute for Cosmological Physics and through an endowment from the Kavli Foundation.

REFERENCES

Amato E., Guetta D., Blasi P., 2003, A&A, 402, 827
Arnett W. D., 1980, ApJ, 237, 541
Arons J., 2002, in Slane P. O., Gaensler B. M., eds, ASP Conf. Ser. Vol. 271, Neutron Stars in Supernova Remnants. Astron. Soc. Pac., San Francisco, p. 71
Arons J., 2003, ApJ, 589, 871
Arons J., 2007, preprint (arXiv:0708.1050)
Baklanov P. V., Blinnikov S. I., Pavlyuk N. N., 2005, Astron. Lett., 31, 429
Bandiera R., Pacini F., Salvati M., 1984, ApJ, 285, 134
Begelman M. C., Li Z.-Y., 1992, ApJ, 397, 187
Bennett L., Ellison D. C., 1995, J. Geophys. Res., 100, 3439
Bhattacharya D., 1990, J. Astrophys. Astron., 11, 125
Bietenholz M. F., Bartel N., Rupen M. P., 2010, ApJ, 712, 1057
Blasi P., Epstein R. I., Olinto A. V., 2000, ApJ, 533, L123
Bucciantini N., Arons J., Amato E., 2011, MNRAS, 410, 381
Chatzopoulos E., Wheeler J. C., Vinko J., 2012, ApJ, 746, 121
Chen P., Tajima T., Takahashi Y., 2002, Phys. Rev. Lett., 89, 161101
Chevalier R. A., 1977, in Schramm D. N., ed., Astrophysics and Space Science Library Vol. 66, Supernovae. Reidel, Dordrecht, p. 53
Chevalier R. A., 2005, ApJ, 619, 839
Chevalier R. A., Fransson C., 1992, ApJ, 395, 540
Contopoulos I., Kazanas D., 2002, ApJ, 566, 336
Del Zanna L., Amato E., Bucciantini N., 2004, A&A, 421, 1063
Del Zanna L., Volpi D., Amato E., Bucciantini N., 2006, A&A, 453, 621
Dessart L., Hillier D. J., Waldman R., Livne E., Blondin S., 2012, 426, L76
Dieckmann M. E., Bret A., 2009, ApJ, 694, 154
Emmering R. T., Chevalier R. A., 1987, ApJ, 321, 334
Fang J., Zhang L., 2010, A&A, 515, A20
Fang K., Kotera K., Olinto A. V., 2012, ApJ, 750, 118
Fang K., Kotera K., Olinto A. V., 2013, J. Cosmol. Astropart. Phys., 3, 10
Faucher-Giguère C.-A., Kaspi V. M., 2006, ApJ, 643, 332
Gaensler B. M., Slane P. O., 2006, ARA&A, 44, 17
Gaffet B., 1977a, ApJ, 216, 565
Gaffet B., 1977b, ApJ, 216, 852
Gelfand J. D., Slane P. O., Zhang W., 2009, ApJ, 703, 2051
Hamuy M., 2003, ApJ, 582, 905
Kasen D., Bildsten L., 2010, ApJ, 717, 245
Kasen D., Woosley S. E., 2009, ApJ, 703, 2205
Katz B., Sapir N., Waxman E., 2011, preprint (arXiv:1106:1898)
Kennel C. F., Coroniti F. V., 1984a, ApJ, 283, 694
Kennel C. F., Coroniti F. V., 1984b, ApJ, 283, 710
Kirk J. G., Lyubarsky Y., Petri J., 2009, in Becker W., ed., Astrophysics and Space Science Library Vol. 421, Neutron Stars and Pulsars. Springer, Berlin, p. 421
Komissarov S., Lyubarsky Y., 2004, Ap&SS, 293, 107
Lyubarsky Y. E., 2003, MNRAS, 345, 153
McCray R., Shull J. M., Sutherland P., 1987, ApJ, 317, L73
Matzner C. D., McKee C. F., 1999, ApJ, 510, 379
Murase K., Mészáros P., Zhang B., 2009, Phys. Rev. D, 79, 103001
Murase K., Thompson T. A., Lacki B. C., Beacom J. F., 2011, Phys. Rev. D, 84, 043003
Otsuka M. et al., 2012, ApJ, 744, 26
Pacini F., Salvati M., 1973, ApJ, 186, 249
Pétri J., Lyubarsky Y., 2007, A&A, 473, 683
Quimby R. M., 2012, in Proc. IAU Symp. 279, Death of Massive Stars: Supernovae and Gamma-Ray Bursts. Cambridge Univ. Press, Cambridge, p. 22
Rees M. J., Gunn J. E., 1974, MNRAS, 167, 1
Rest A. et al., 2011, ApJ, 729, 88
Reynolds S. P., Chevalier R. A., 1984, ApJ, 278, 630
Shapiro S. L., Teukolsky S. A., 1983, Black Holes, White Dwarfs, and Neutron Stars: The Physics of Compact Objects. John Wiley and Sons, New York
Sironi L., Spitkovsky A., 2009, ApJ, 707, L92
Spitkovsky A., 2008, ApJ, 682, L5
Srinivasan G., Dwarakanath K. S., Bhattacharya D., 1984, J. Astrophys. Astron., 5, 403
Svirski G., Nakar E., Sari R., 2012, ApJ, 759, 108
Tanaka S. J., Takahara F., 2011, ApJ, 741, 40
Utrobin V. P., Chugai N. N., 2008, A&A, 491, 507
Weiler K. W., Panagia N., 1980, A&A, 90, 269
Woosley S. E., Heger A., Weaver T. A., 2002, Rev. Mod. Phys., 74, 1015
Xu Y., Sutherland P., McCray R., Ross R. R., 1988, ApJ, 327, 197

This paper has been typeset from a TEX/LATEX file prepared by the author.